Optical Engineering

OpticalEngineering.SPIEDigitalLibrary.org

# Synchronous optical sampling with chirped optical pulse based on high nonlinear spiral photonic crystal fiber

Sha Li
Jianping Wang
Zhiguo Shi
Xianting Zhang
Zhe Kang
Chongxiu Yu

SPIE.

# Synchronous optical sampling with chirped optical pulse based on high nonlinear spiral photonic crystal fiber

**Sha Li,[a,*] Jianping Wang,[a] Zhiguo Shi,[a] Xianting Zhang,[a] Zhe Kang,[b] and Chongxiu Yu[b]**
[a]University of Science and Technology Beijing, Electrical and Mechanical Services Building 727, Haidian District, Beijing 100083, China
[b]Beijing University of Posts and Telecommunications, State Key Laboratory of Information Photonics and Optical Communications, Beijing 100876, China

**Abstract.** We optimize a proposed multicast parametric synchronous sampling scheme. Two segments of 1 cm high nonlinear spiral photonic crystal fiber are utilized as a nonlinear medium in parametric processors. Meanwhile, a segment of 1.8 km dispersion compensation fiber is used to obtain linear chirped sampling pulses instead of a 5 km single-mode fiber. The experimental results show that a 120 GSa/s equivalent sampling rate, high power of sampling copies, and low variance are obtained.  [DOI: 10.1117/1.OE.54.5.055105]

Keywords: analog-to-digital conversion; photonic crystal fiber; signal multicast; linear chirped pulse.

Paper 150347 received Mar. 18, 2015; accepted for publication May 5, 2015; published online May 22, 2015.

## 1 Introduction

Analog-to-digital convertor (ADC) as an important part of communication systems needs to satisfy requirements of the rapid development of ultrawide-band applications such as advanced Radar communication systems, high-speed optical communication, and so on.[1–3] The electrical ADC whose sample rate is only several gage-samples per second (GSa/s) cannot meet the requirements of ultrawide-band applications because of its inherent electrical bottle-neck such as clock jitter and sampling aperture.[1–4] Optical signal processing has attracted researchers' interests because it can overcome the electrical limitations.[5–8] Bres et al.[9] demonstrated a 320 Gb/s optical demultiplexing sampling method that required a mode-locked laser with a very high repetition rate. In order to meet the requirement, a large number of copies are needed. Zhang et al.[10] proposed a multicast parametric synchronous optical sampling scheme using only three copies based on a high nonlinear fiber (HNLF). However, a fiber length over 200 m was used to realize all-optical ADC, which is disadvantageous for photonics integration.

In this paper, we optimize a proposed multicast parametric synchronous sampling scheme utilizing a 2 cm high nonlinear spiral photonic crystal fiber (PCF) instead of a 200 m HNLF as the nonlinear medium based on the parametric process and a 1.8 km dispersion compensation fiber (DCF) instead of the 5 km single-mode fiber (SMF) as the time-stretched medium, respectively. The experimental results show the parametric process efficiency based on a high nonlinear spiral PCF and verify the feasibility of our optimized scheme.

## 2 Theory of Operation

The scheme is composed of signal multicast, time delay, and parametric sampling blocks. The original signal as the pump is copied utilizing a parametric process in a high nonlinear spiral $PCF_1$. The idler gain is

$$G \propto \exp[2\gamma L E_p(t)], \tag{1}$$

where $\gamma$ is the nonlinear coefficient, $L$ is the fiber length, and $E_p(t)$ is the pump power. The idlers change with the original pump to realize signal multicast.

In order to temporally overlap the pulse center of the pump and a nonreturn-to-zero (NRZ) code, these idlers are fed into an SMF to temporally delay each other by a factor

$$\Delta\tau = T_{\mathrm{NRZ}}/3, \tag{2}$$

where $\Delta\tau$ is the temporal delay and $T_{\mathrm{NRZ}}$ is the period of the NRZ signal. Hence, the temporal delays are $-\Delta\tau$, 0, and $+\Delta\tau$ between the pump and idler 1, idler 2, and idler 3, respectively.

Time-stretched and linearly chirped pulses are used as the sampling pump signal based on high nonlinear spiral $PCF_2$ in a parametric sampling block. The pump pulses are fed into a DCF to obtain linear chirp.[11,12] The linear chirped pulses are delivered into a high nonlinear spiral $PCF_2$ with idlers as $A_{i,n}(t)$ $(n = 1,2,3)$. The phases of sampling copies given as $A_{\mathrm{sc},n}(t)$ $(n = 1,2,3)$ are modulated by chirped pump pulses due to phase combination between pump and idlers in the high nonlinear spiral $PCF_2$. The gain frequency variation of the sampling copies is

$$\delta\omega_{\mathrm{sc}}(T) = -2\frac{\partial\phi_p}{\partial T} = \frac{2\mathrm{sgn}(\beta_2)(z/L_D)}{1+(z/L_D)^2}\frac{T}{T_0^2}, \tag{3}$$

where $\phi_p$ is the phase of the chirped pump pulse, $\beta_2$ and $L_D$ are the group velocity dispersion and the dispersion length of high nonlinear spiral $PCF_2$, respectively, and $T_0$ is the full width at half maximum.[13–16] From Eq. (3), the chirp of the pump can be transferred to sampling copies and the chirp of sampling copies is twice that of the pump. Therefore, an arrayed waveguide grating (AWG) is utilized to extract different frequency components of the sampling copies. Finally, the sampling time points are sent into a

*Address all correspondence to: Sha Li, E-mail: shalee@ustb.edu.cn

data signal processing module to realize quantization and coding. In the sampling scheme, the equivalent sampling rate is

$$R_s = \frac{|\delta\omega_{sc}(T)|_{max} n R_{pump}}{\Delta f}, \quad (4)$$

where $n$ is the number of copies, $R_{pump}$ is the repetition rate of the pump, and $\Delta f$ is the bandwidth of the filters. If the bandwidth of the filters is a constant, a larger chirp of the sampled copies supports a higher equivalent sampling rate. Hence, a high equivalent sampling rate can be achieved when the pump rate is far below the Nyquist rate.

## 3 Results and Discussion

Based on the above theoretical analysis, we optimize the proposed multicast parametric synchronous sampling scheme utilizing a high nonlinear spiral PCF as the nonlinear processing medium. The optimized schematic diagram is exhibited in Fig. 1. First, the degenerated pump signal with 1550.4 nm center wavelength is phase modulated by 50, 150, and 300 MHz radio frequency harmonics to suppress stimulated Brillouin scattering. Next the pump signal is amplitude modulated by 10 Gb/s NRZ bit sequence. Then the pump signal is amplified by erbium-doped fiber amplifier ($EDFA_1$) and filtered by an optical bandpass filter ($BPF_1$) with a 0.6 nm bandwidth to eliminate the amplified spontaneous emission noise, respectively. Subsequently, the amplified pump signal is coupled into a 1 cm high nonlinear spiral $PCF_1$ with three continuous waves (CWs) whose peak powers are 1 dBm and whose center wavelengths are 1558.8, 1560.8, and 1562.8 nm for signal multicast. Three idlers are delivered into a 1.2 km SMF to realize a temporal delay with each other after optical $BPF_2$ that removes the pump signal and three CWs at the output of $PCF_1$. Ten gigahertz Gaussian optical pulses with a 1555 nm center wavelength and 10 ps pulse width are delivered into 1.8 km DCF instead of a 5 km SMF to stretch in time domain and gain linear chirp and are amplified by $EDFA_2$. The amplified pulses as the sampling pulse train are coupled into $PCF_2$ with the three idlers for parameter processing. Finally, the different frequencies are separated by an AWG, and a digital signal processor (DSP) realizes photoelectric conversion, quantization, and coding.

In our system, the 2 cm high nonlinear spiral PCF is utilized as a nonlinear medium instead of the 200 m HNLF. Its structure is shown in Fig. 2(a). The spiral PCF consists of an elliptical slot core with a low index silicon nanocrystals (Si-nc) rod surrounded by three rings of air holes in a spiral lattice. The PCF has six spiral arms, where each arm shapes a single spiral with $r$ radius and $\theta$ angular increment. The curves of the dispersion and the nonlinear coefficient of the fundamental mode versus the wavelength are shown in Fig. 2(b). Based on the spiral structure, the dispersion is only $-0.07\ \mathrm{ps/(nm \cdot km)}$ and the dispersion slope is $-1.25 \times 10^{-3}\ \mathrm{ps/(nm^2 \cdot km)}$ at the wavelength of 1550 nm. The nonlinear coefficients of the fundamental mode are as high as $224.36\ \mathrm{W^{-1}\,m^{-1}}$ and are $1.87 \times 10^4$ times as large as the one of the HNLF.[17–19]

The spectra at the outputs of $PCF_1$ and $PCF_2$ are recorded as shown in Figs. 3(a) and 3(b) together with the eye diagrams of idler 1 and copy 1 (insets), respectively. The three idlers are generated at 1538.01, 1540.09, and 1541.98 nm with approximately the same peak power in Fig. 3(a), and further optical processing is conveniently based on the same peak power for each NRZ code. As

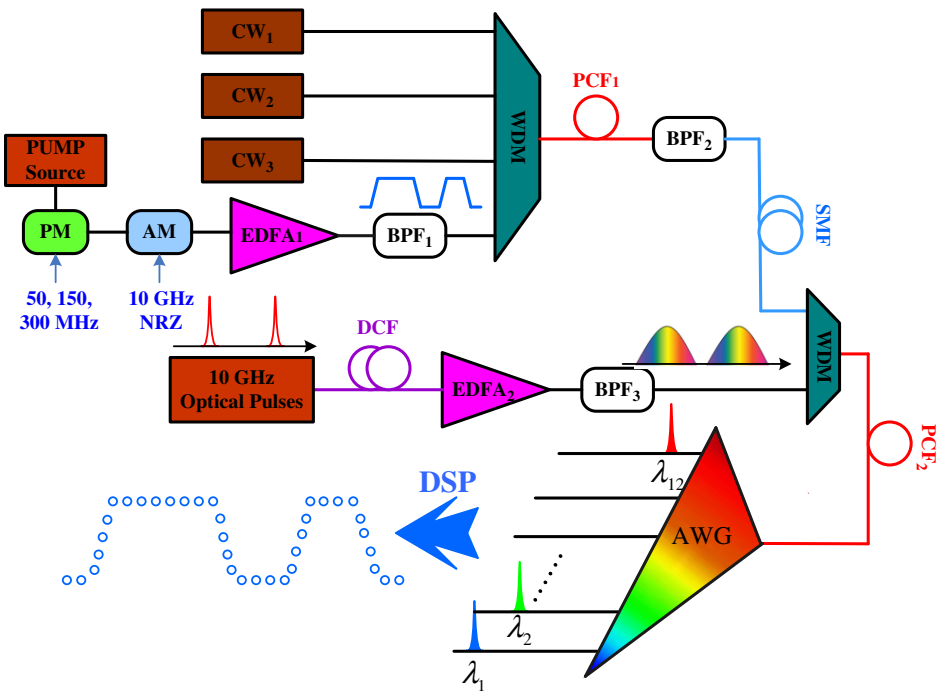


**Fig. 1** Schematic diagram of the optimized scheme. CW: continuous wave, PM: phase modulation, AM: amplitude modulation, EDFA: erbium-doped fiber amplifier, BPF: bandpass filter, WDM: wavelength division multiplexer, PCF: photonic crystal fiber, DCF: dispersion compensation fiber, AWG: arrayed waveguide grating, DSP: digital signal processor.

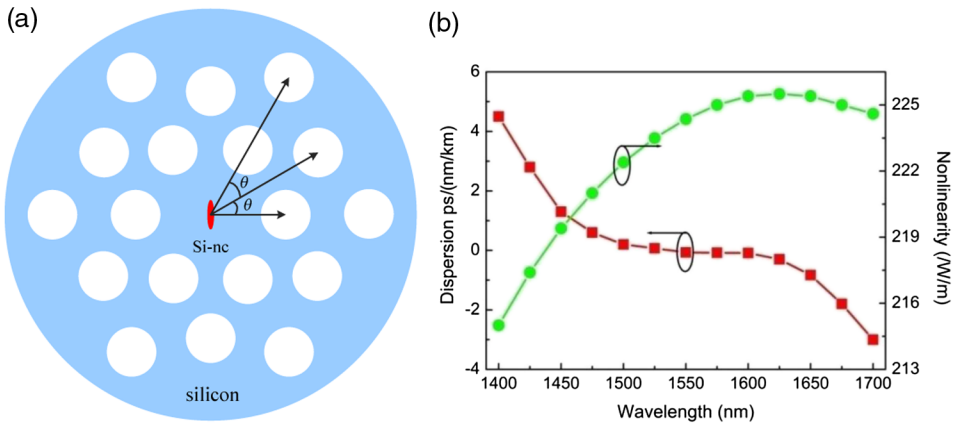


**Fig. 2** The spiral PCF: (a) structural diagram of the high nonlinear spiral PCF; (b) dispersion and nonlinearity versus wavelength curves.

shown in Fig. 3(b), three sampling copies are generated at 1568.22, 1570.20, and 1572.21 nm and the maximum peak power is −5.235 dBm at 1570.20 nm. The simulation results are in very good agreement with the measurements. The spectrum widths of the three sampling copies are wider than the ones of the three idlers, which means the chirp of the pump transfers to the sampling copies. According to the above theoretical analysis, the chirp of the sampling copies is twice that of the pump. So the sampling copies can be filtered by an AWG with a 0.2 nm bandwidth and 12 wavelengths from 1567.91 to 1572.66 nm.

To ensure the same time interval for all of the samples and extract precisely different temporal sampling points, we chose 12 sampling channels as shown in Table 1. The peak powers of 12 sampling channels utilizing a 2 cm high nonlinear spiral PCF as a nonlinear medium after the photoelectric detector are recorded and compared with the ones utilizing a 200 m HNLF. There are peak power variations among samples whether PCF or HNLF is utilized as the nonlinear medium, because of the irregular amplitude of time-stretched sampling pulses and the gain ripples of sampled copies. As shown in Table 1, the peak powers using PCF as a nonlinear medium are higher than the ones using HNLF, where the maximum and minimum deviations are 15.84 and 31.01 dB, respectively. Because the spiral PCF has a very high nonlinear coefficient, the idlers with high peak power are easily obtained.

Subsequently, these electrical signals are sent into the signal processing block for equalization. The distortion of

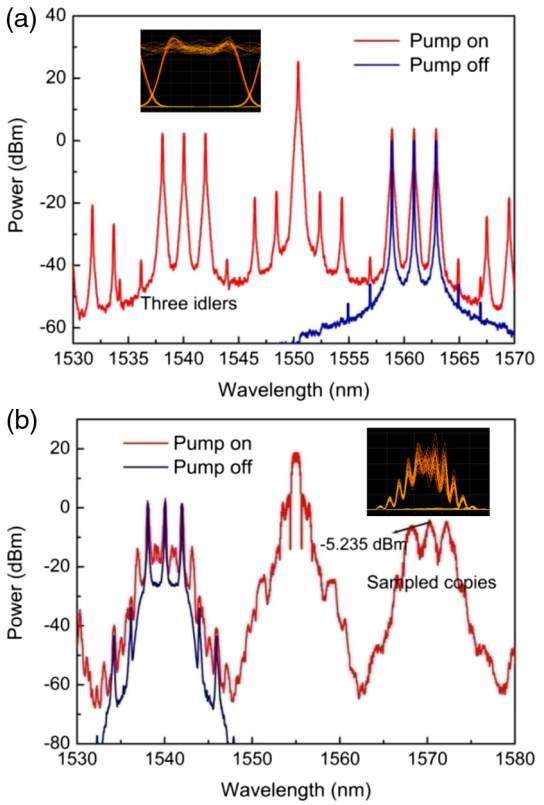


**Fig. 3** Spectral profiles (a) at output of $PCF_1$ and (b) at output of $PCF_2$ with pump on and off. Insets: the eye diagrams of idler 1 and copy 1.

**Table 1** Sampling performance.

| Sampling channel | Center wavelength (nm) | Peak power (dBm) (2 cm PCF) | Peak power (dBm) (200 m HNLF) |
|---|---|---|---|
| 1 | 1567.91 | −46.86 | −65.88 |
| 2 | 1568.14 | −48.06 | −63.90 |
| 3 | 1568.35 | −33.28 | −54.71 |
| 4 | 1568.60 | −23.80 | −53.98 |
| 5 | 1569.86 | −19.09 | −46.72 |
| 6 | 1570.10 | −30.32 | −56.87 |
| 7 | 1570.37 | −31.91 | −54.92 |
| 8 | 1570.63 | −19.99 | −46.33 |
| 9 | 1571.86 | −14.45 | −42.81 |
| 10 | 1572.18 | −29.69 | −56.77 |
| 11 | 1572.38 | −31.46 | −53.11 |
| 12 | 1572.66 | −25.41 | −56.42 |

Note: PCF, photonic crystal fiber; HNLF, high nonlinear fiber.

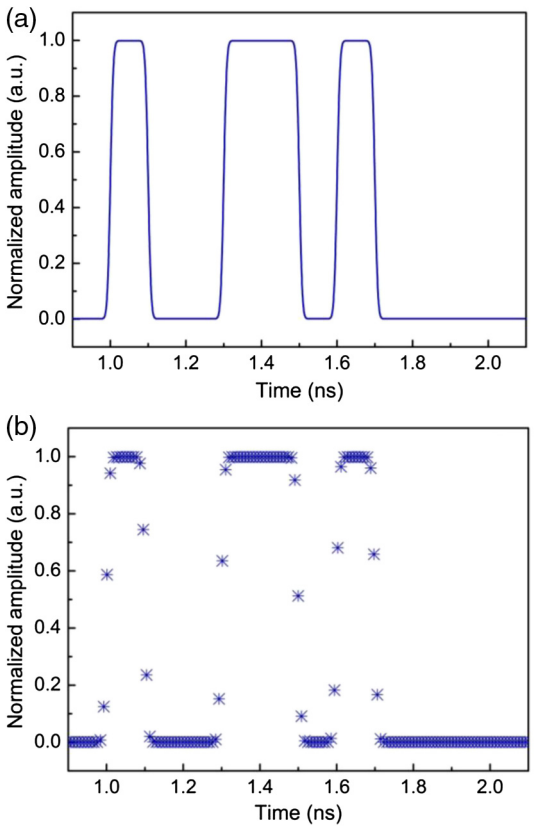


**Fig. 4** (a) Original 10 Gb/s nonreturn-to-zero (NRZ) signal. (b) Sampling points of original waveform with 120 GSa/s.

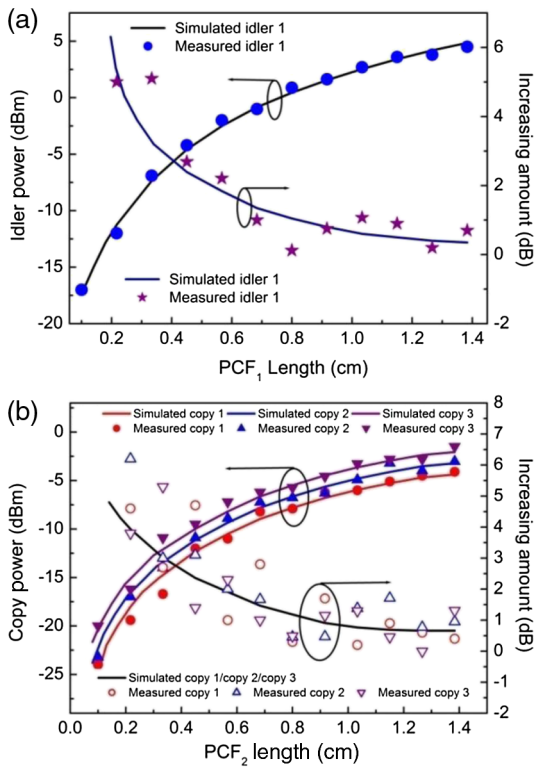


**Fig. 5** Power of the idler 1 and sampling copies and their increasing amount as the function of fiber length: (a) at the output of $PCF_1$; (b) at the output of $PCF_2$, $L_{PCF_1} = 1$ cm.

sampling can be eliminated from the shape of the linearly chirped pump and the gain ripples. In the DSP, the equalization function is

$$S = (e_1, e_2 \cdots e_{12}) \begin{pmatrix} s_1 & & 0 \\ & \ddots & \\ 0 & & s_{12} \end{pmatrix}, \tag{5}$$

where $S$ is the final sampling time points, $s_1, s_2, \ldots, s_{12}$ are the sampling points, and $e_1, e_2, \ldots, e_{12}$ are the equalization coefficients. The amplitude of the original signal is set as a constant, then the equalization coefficients are determined. In the DSP, the electrical signals are processed at the rate of 10 Gb/s. Such a processing rate corresponds to the repetition rate of the original laser source and is quite within the speed, which is compatible with electronic devices. The original signal and equalized sampling points are shown in Figs. 4(a) and 4(b), respectively. It is evident that the sampling points are in good agreement with the original signal with an equivalent sample rate of 120 GSa/s.

Changing the length of the PCF will induce different gain ripples and this will induce sampling distortion. The powers of the idler 1 and copies as a function of the length of $PCF_1$ and $PCF_2$ are recorded in Figs. 5(a) and 5(b), respectively. The power of the idler 1 and three sampling copies increases with the lengths of $PCF_1$ and $PCF_2$, respectively. The simulation results are in very good agreement with the experimental data. The powers of the three idlers are almost the

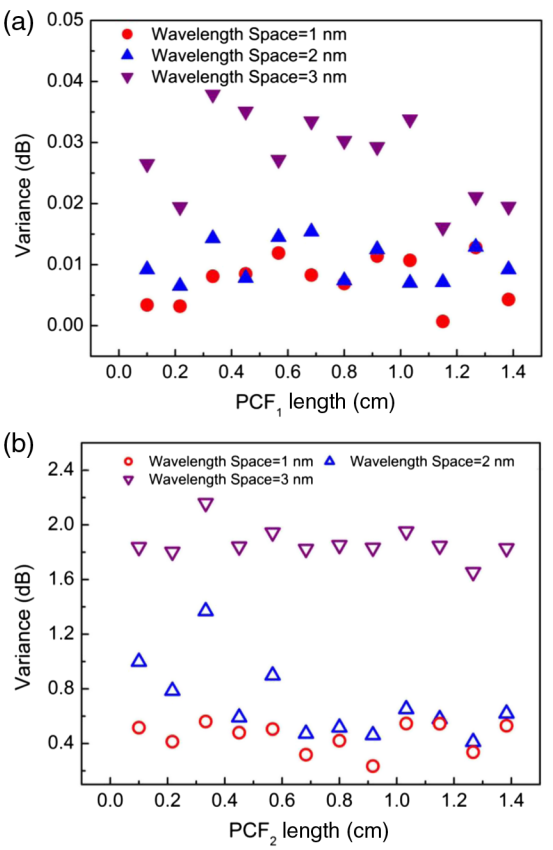


**Fig. 6** Different wavelength space between each CW effect on the variance: (a) the length of $PCF_1$ versus the variance curves; (b) the length of $PCF_2$ versus the variance curves.

same at the output of $PCF_1$, but there are power variations among the three sampling copies at the output of $PCF_2$ due to the irregular shape of the sampling pulses. With the increase in the length of $PCF_1$ and $PCF_2$, the power increasing amount of idlers and copies decreases monotonically and approaches zero, respectively. Consequently, it is inadvisable that high power for idlers or copies be obtained by increasing the fiber length.

The sampling distortion comes not only from the fiber length, but also the wavelength space between each CW. Here, we define the variance as

$$\text{variance} = \frac{1}{3}\left[\sum_{i=1}^{3}(\text{power}_i - \text{average})^2\right]^{1/2}, \quad (6)$$

where $\text{power}_i$ is the power of idler $i$ or sampling copy $i$ $(i = 1,2,3)$, and $\text{average} = 1/3\sum_{i=1}^{3}\text{power}_i$. The lengths of $PCF_1$ and $PCF_2$ versus the variances diagrams with different wavelength space are recorded in Figs. 6(a) and 6(b), respectively. With the increase in the length of $PCF_1$ or $PCF_2$, the variance value gets a random jitter. Figure 6(a) shows that the variance becomes large when the wavelength space between each CW is 3 nm. This is because the power of the idlers depends on the wavelength conversion efficiency of the CWs, which changes with the center wavelength of each CW.[20] When the wavelength space between each CW is 3 nm, the maximal variance is 0.037 dB at the output of $PCF_1$.

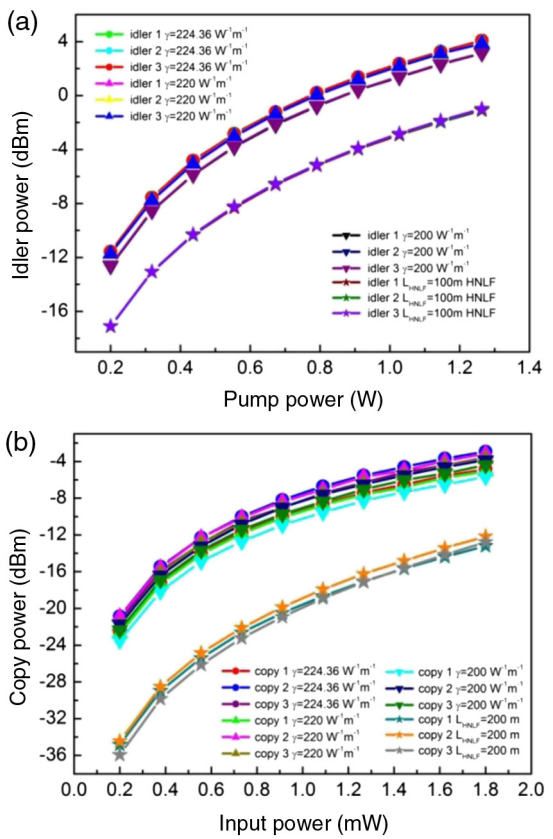


**Fig. 7** Different input peak powers of pump and sampling pulses effect on the powers of idlers and sampling copies: (a) input peak powers of pump versus powers of idlers curves with different nonlinear coefficients; (b) input peak powers of sampling pulses versus powers of copies curves with different nonlinear coefficients.

When the length of $PCF_1$ is 1 cm, the variance gets large with the increase in the wavelength space as shown in Fig. 6(b). Due to the gain ripples of the idlers and the irregular shape of the sampling pulse, the variance at the output of $PCF_2$ is larger than the one at the output of $PCF_1$. When the wavelength space between each CW is 3 nm, the maximal variance is 2.159 dB at the output of $PCF_2$. However, the minimal variance at the output of $HNLF_1$ is 0.6 dB in the previous scheme when the wavelength space is 3 nm, leading to a large sampling distortion.

Changing the power of the pump or sampling pulse will also induce different gain ripples and this will also induce sampling distortion. The power of idlers and sampling copies versus the input power of pump and sampling pulse diagrams with different nonlinear coefficients is simulated, as shown in Figs. 7(a) and 7(b), respectively. The power of idlers or sampling copies monotonously increases and slopes gently with the increase in the input power of the pump or sampling pulse in any case of nonlinear coefficient $\gamma$. In Fig. 7(a), the curves are fitted with the same nonlinear coefficient $\gamma$, and the power of idlers is higher by 4.51 dB than the one utilizing HNLF as a nonlinear medium. In Fig. 7(b), the curves have a deviation with the same nonlinear coefficient $\gamma$ due to the gain ripples of idlers and the irregular shape of the sampling pulse; the power of the sampled copies is 12.44 dB higher than the one utilizing HNLF as a nonlinear medium.

## 4 Conclusion

In summary, we optimize a proposed multicast parametric synchronous sampling scheme utilizing 2 cm high nonlinear spiral PCF instead of 200 m HNLF as nonlinear medium based on parametric process and 1.8 km DCF instead of 5 km SMF as time-stretched medium, respectively. By using the high nonlinear spiral PCF, the high power of sampling copies and low variance are obtained to avoid sampling distortion. In order to realize real-time sampling and reduce the requirements of the electronic devices, the chirped sampling pulses are utilized and a 120 GSa/s equivalent sampling rate is obtained. Compared with the pre-existing schemes, the size of the parametric processor can be much smaller than those previously proposed based on HNLF. Therefore, our optimized scheme is more in line with the concept of integration and miniaturization.

### *Acknowledgments*

This work is jointly supported by Beijing Natural Science Foundation under Grant No. 4122049, Beijing Higher Education Young Elite Teacher (No. YETP0381), and the Fundamental Research Funds for the Central Universities (FRF-JX-12-002, FRF-TP-12-083A, and FRF-TP-14-049A2).

### *References*

1. A. Khilo, S. J. Spector, and M. E. Grein, "Photonic ADC: overcoming the bottleneck of electronic jitter," *Opt. Express* **20**(4), 4454 (2012).
2. K. Zhe, Y. Jin-Hui, and L. Sha, "Six-bit all-optical quantization using photonic crystal fiber with soliton self-frequency shift and pre-chirp spectral compression techniques," *Chin. Phys. B* **22**(11), 114211 (2013).
3. K. Xu et al., "All-optical analog-to-digital conversion scheme based on Sagnac loop and balanced receivers," *Appl. Opt.* **50**, 1995–1999 (2011).
4. G. C. Valley, "Photonic analog-to-digital converters," *Opt. Express* **15**(5), 1955–1982 (2007).

5. Z. Kang et al., "Lumped time-delay compensation scheme for coding synchronization in the nonlinear spectral quantization-based all-optical analog-to-digital conversion," *IEEE Photonics J.* **5**(6), 7201109 (2013).
6. Z. Kang et al., "Six-bit all-optical quantization employing photonics crystal fiber based soliton self-frequency shift and pre-chirp spectral compression technique," *Chin. Phys. B* **22**, 114211 (2013).
7. D. Tang et al., "Ultrashort optical pulse monitoring using asynchronous optical sampling technique in highly nonlinear fiber," *Chin. Opt. Lett.* **8**(7), 630–633 (2010).
8. M. Westlund et al., "High-performance optical-fiber-nonlinearity based optical waveform monitoring," *J. Lightwave Technol.* **23**(6), 2012–2022 (2005).
9. C.-S. Bres et al., "Multicast parametric synchronous sampling," *IEEE Photonics Technol. Lett.* **20**(14), 1222–1224 (2008).
10. X. Zhang et al., "Scheme for multicast parametric synchronous optical sampling," *Opt. Eng.* **53**(5), 056102 (2014).
11. Y. Han, O. Boyraz, and B. Jalali, "480 GSample/s time stretch transient digitizer," in *IEEE: TIMC 2004-Lightwave Technologies in Instrumentation & Measurement Conference Palisades*, New York (2004).
12. Y. Han and B. Jalali, "Photonic time-stretched analog-to-digital converter: fundamental concepts and practical considerations," *Lightwave Technol.* **21**(12), 3085–3103 (2003).
13. G. P. Agrawal, *Nonlinear Fiber Optics*, 4th ed., Elsevier, Amsterdam (2007).
14. H. C. H. Mulvad et al., "Ultra-high-speed optical serial-to-parallel data conversion by time-domain optical Fourier transformation in a silicon nanowire," *Opt. Express* **19**(26), B825–B835 (2011).
15. E. Palushani et al., "OTDM-to-WDM conversion based on time-to frequency mapping by time-domain optical Fourier transformation," *IEEE J. Sel. Top. Quantum Electron.* **18**(2), 681–688 (2012).
16. R. Salem et al., "High-speed optical sampling using a silicon-chip temporal magnifier," *Opt. Express* **17**(6), 4324–4329 (2009).
17. J. Liao et al., "Highly nonlinear dispersion-flattened slotted spiral photonic crystal fibers," *Photonics Technol. Lett.* **26**(4), 380–383 (2014).
18. M. Ebnali-Heidari et al., "Proposal for supercontinuum generation by optofluidic infiltrated photonic crystal fibers," *IEEE J. Sel. Top. Quantum Electron.* **20**(5), 7500408 (2014).
19. H. Chen et al., "All-fiber-integrated high-power supercontinuum sources based on multi-core photonic crystal fibers," *IEEE J. Sel. Top. Quantum Electron.* **5**(20), 0902008 (2014).
20. J. Hansryd et al., "Fiber-based optical parametric amplifiers and their applications," *IEEE J. Sel. Top. Quantum. Electron.* **8**(3), 506–520 (2002).



**Sha Li** received her PhD in optical engineering at Beijing University of Posts and Telecommunications (BUPT), Beijing, China, in 2014. She is currently a postdoctoral researcher in School of Computer and Communication Engineering, University of Science and Technology Beijing (USTB), Beijing, China. Her research interests include optical signal processing, all-optical analog-to-digital conversion, and nonlinear fiber optics.

**Jianping Wang** is now the vice president in School of Computer and Communication Engineering, University of Science and Technology Beijing (USTB), Beijing, China. She has published more than 50 papers, of which more than 20 articles were in SCI. Her current research interests include optical signal processing, visible light communication, and deep space communication.

Biographies for the other authors are not available.